ANTIOXIDANTS & REDOX SIGNALING
Volume 6, Number 3, 2004

Forum Original Research Communication

In Situ Reduction of Oxidative Damage, Increased Cell Turnover, and Delay of Mitochondrial Injury by Overexpression of Manganese Superoxide Dismutase in a Multistage Skin Carcinogenesis Model

TERRY D. OBERLEY,[1,2] YI XUE,[2] YUNFENG ZHAO,[3] KELLEY KININGHAM,[3] LUKE I. SZWEDA,[4] and DARET K. ST. CLAIR[3]

ABSTRACT

To study early subcellular pathologic changes of tumorigenesis in mouse skin and possible modulation by overexpression of the mitochondrial antioxidant enzyme manganese superoxide dismutase (MnSOD), skin keratinocytes from nontransgenic (Ntg) and transgenic (TgH) mice overexpressing MnSOD topically treated with one dose of 7,12-dimethylbenz(*a*)anthracene (DMBA) and a subsequent dose of 12-*O*-tetradecanoylphorbol 13-acetate (TPA) were analyzed *in situ* for levels of MnSOD and the oxidative damage product 4-hydroxy-2-nonenal (4HNE)-modified proteins using specific antibodies and immunogold electron microscopy. At all selected time points analyzed after TPA treatment, there was more MnSOD immunoreactive protein in mitochondria of keratinocytes of TgH mice than Ntg mice. Compared with untreated groups, there was a large increase in 4HNE-modified proteins at 6–24 h after TPA treatment, and this increase was larger in Ntg than TgH mice. Indices of mitosis and apoptosis of keratinocytes were greater in DMBA/TPA-treated TgH than Ntg mouse skin. Mitochondrial injury detected by transmission electron microscopy was delayed in keratinocytes of TgH compared with Ntg mice. The present study demonstrated that overexpression of MnSOD not only protected cells from oxidative damage, but also affected cell turnover kinetics. Thus, previously identified reduction in papilloma formation observed in TgH mice is correlated with mitochondrial events. *Antioxid. Redox Signl.* 6, 537–548.

INTRODUCTION

A MULTISTAGE CARCINOGENESIS MODEL has been used to study skin tumor formation in the mouse for many years (4). Stages of carcinogenesis in this model have been defined as initiation, promotion, and progression. 7,12-Dimethylbenz(*a*)anthracene (DMBA) has been used as a tumor initiator, and 12-*O*-tetradecanoylphorbol 13-acetate (TPA) has often been used as a tumor promoter. Whereas DMBA is known to result in DNA damage with subsequent mutations, the role of TPA in tumor promotion is less well understood, even though it has been shown that TPA binds to the enzyme protein kinase C (PKC) and hence regulates phosphorylation within cells (12). The biologic role of PKC in tumor promotion is postulated to be clonal expansion of initiated epidermal cells (23).

TPA may have other biochemical roles in tumor promotion. Keratinocytes treated with TPA *in vitro* show increased levels

[1]Pathology and Laboratory Medicine Service, William S. Middleton Veterans Memorial Hospital, Madison, WI.
[2]Department of Pathology and Laboratory Medicine, University of Wisconsin Medical School, Madison, WI.
[3]Graduate Center for Toxicology, University of Kentucky, Lexington, KY.
[4]Department of Physiology and Biophysics, Case Western Reserve University School of Medicine, Cleveland, OH.

of reactive oxygen species (ROS) (31), and superoxide dismutase (SOD) mimetics, which reduce levels of superoxide anion, have been shown to reduce skin papilloma formation following DMBA/TPA treatment (7). ROS have been demonstrated to have physiologic effects in cells at low concentrations, whereas high concentrations of ROS are known to be toxic (24). To study the role of a mitochondrial antioxidant enzyme in papilloma formation, we developed transgenic (TgH) mice that overexpressed human manganese superoxide dismutase (MnSOD), and these TgH mice showed reduced papilloma formation compared with their nontransgenic (Ntg) littermates (39). The mechanism by which the mitochondrial enzyme MnSOD affects papilloma formation is presently not known.

The present study was designed to determine whether topical DMBA/TPA treatment caused oxidative damage *in situ* in mouse skin, to analyze whether mitochondrial overexpression of MnSOD reduced oxidative damage, to determine whether mitochondrial overexpression of MnSOD affected keratinocyte cell turnover following DMBA/TPA treatment, and to define mitochondrial changes in a multistage skin carcinogenesis model. To study oxidative damage, we used a specific antibody to 4-hydroxy-2-nonenal (4HNE)-modified proteins and immunogold electron microscopy with computerized image analysis, a technique we have previously documented to show tight correlation with biochemical assessment of lipid peroxidation (37). This technique allows for the first time an analysis of biochemical events occurring at the subcellular level in keratinocytes of intact mouse skin after DMBA/TPA treatment. We document both nuclear and mitochondrial lipid peroxidation-protein adducts, mitochondrial injury, and amelioration or delay of these changes by overexpression of MnSOD. In addition, we demonstrate that MnSOD overexpression increases cell turnover, both mitosis and apoptosis, in DMBA/TPA-treated skin. Taken together with our recent demonstration of regulation of nuclear transcription factor activator protein-1 (AP-1) activity and p53 levels by MnSOD modulation (39, 41), our results suggest the possibility of mitochondrial-mediated regulation of tumor promotion via mitochondria-to-nucleus signaling events.

MATERIALS AND METHODS

Mice

Human MnSOD TgH mice were generated as previously described (36). In brief, human MnSOD cDNA was introduced into pronuclei of fertilized eggs by microinjection. Mice used for producing TgH mice were the F1 progeny of C57BL/6 mice crossed with C3H hybrid (B6C3) mice that were purchased from Harlan Sprague–Dawley (Indianapolis, IN, U.S.A.). Methods for identification and characterization of TgH mice have been previously reported (36). For skin tumorigenesis experiments, female TgH mice that exhibited a high level of MnSOD activity and their Ntg littermates were used. Previous studies have demonstrated a decrease in papilloma formation in MnSOD-overexpressing female but not male mice (unpublished observations). Therefore, previous published studies characterizing this system used only female mice (39, 41).

Two-stage carcinogenesis

Hair from the backs of 6–8-week-old female mice was shaved prior to application of vehicle dimethyl sulfoxide (DMSO) (Sigma, St. Louis, MO, U.S.A.) or carcinogen. Mice in the resting stage of the hair cycle were used in all experiments. A single dose of 20 n*M* DMBA (Sigma) dissolved in DMSO was painted on each mouse. After 2 weeks, one dose of 4 μg of TPA (Sigma) dissolved in DMSO was applied to the same area; these mice are referred to in the text as "DMBA/TPA" treated mice. Additional groups studied included mice treated with DMSO alone, DMBA dissolved in DMSO (referred to in the text as "DMBA" treated mice), or TPA dissolved in DMSO (referred to in the text as "TPA" treated mice). Mice were euthanized at varying time points after chemical application.

Conventional electron microscopy

Techniques for routine electron microscopy have been previously published (10). In brief, skin tissues were fixed in glutaraldehyde, embedded in Epon, and thin-sectioned with an ultramicrotome; then sections were placed on nickel grids, stained with lead citrate and uranyl acetate, and examined and photographed with a Hitachi H-600 electron microscope.

Immunogold electron microscopy

After euthanasia, skin from each mouse was removed and fixed in Carson–Millonig's fixative. Carson–Millonig's fixative was used because of its well-known ability to preserve antigenicity. Procedures for immunogold labeling of tissues with antibodies to MnSOD or 4HNE-modified proteins have been previously described (26, 28, 29, 38). Fixed tissues were embedded in LR White resin. LR White-embedded tissue blocks were trimmed and sectioned. Thin sections were mounted on 1% collodion membrane-coated nickel grids. Sections were rinsed and treated with a 0.5% solution of bovine serum albumin in phosphate-buffered saline, pH 7.4, for 30 min to block nonspecific staining and then incubated with primary antibody at 4°C overnight. Rabbit polyclonal anti-human MnSOD (a gift from Dr. Larry Oberley, University of Iowa) was used at a dilution of 1:200, whereas rabbit polyclonal anti-4HNE-modified proteins (from Dr. Luke Szweda, Case Western Reserve University) were used at a dilution of 1:60. The latter antibody was directed against 4HNE bound to keyhole limpet hemocyanin and recognizes the hemiacetal form of the 4HNE-derived portion of protein–4HNE adducts (5). After incubation with primary antibody overnight at 4°C, grids were rinsed in four changes of Tris-buffered saline (TBS) washing buffer for 5 min each and one change of alkaline TBS for 20 min. The grids were then incubated with diluted (1:75) gold-conjugated secondary antibody (gold-conjugated goat anti-rabbit IgH+L, GAR15, BB International, Cardiff, U.K.) for 90 min at room temperature. The sections were washed in two changes of distilled water, and the grids were counterstained with 7.5% uranyl acetate, and observed and photographed with a Hitachi H-600 transmission electron microscope. For each antibody studied, all of the sections for quantitative immunogold electron microscopy analysis for each experiment were stained simultaneously under the same conditions.

Analysis of cell turnover in keratinocytes of interfollicular epidermis

Mitosis and apoptosis were counted in LR White-embedded thick sections from the same skin tissues that were analyzed for MnSOD immunoreactive protein by immunogold ultrastructural analysis. Skin is composed of hair follicles with associated follicular epidermis and epidermis between hair follicles (interfollicular epidermis). Skin tumors have been shown to arise in both follicular and interfollicular epidermis (11, 35), but the specific site of tumor formation in the hair follicle is not certain (22). To avoid the latter controversy, we decided to study interfollicular epidermis only. Thus, cell turnover was analyzed in the interfollicular epidermis. Thick sections of epidermis from each mouse were analyzed for mitosis or apoptosis using morphologic criteria. Mitosis was defined using standard criteria for identification of various mitotic stages: prophase, metaphase, anaphase, telophase, and cytokinesis. Apoptosis was defined by the presence of chromatin condensation, cell shrinkage, and the formation of apoptotic bodies. Conventional electron microscopy was performed to confirm that light microscopy results were accurate by also identifying apoptosis and mitosis using ultrastructural criteria. Three blocks from each mouse were trimmed, and thick sections (0.5 μm) were analyzed with a light microscope. Five hundred cells from each block at each time point were counted (1,500 total cells), and results expressed as a percentage of apoptosis or mitosis per total cells.

Quantitative analysis of MnSOD immunoreactive protein and immunoreactive 4HNE-modified proteins

Micrographs were randomly taken at 10,000× magnification from whole epidermis (in areas where the epidermis was thin) or from an equal number of keratinocytes from stratum germinativum (squamous layer), stratum spinosum (granular layer; characterized by frequent desmosomes, keratohyaline granules, and tonofibrils), and basal cells of the epidermis (the latter analysis performed in areas of the skin that were thick). Nonkeratinocytes, stratum corneum, and cells of the hair follicle were not included in the analysis. The area of mitochondria, cytoplasm, and nucleus in selected epidermal cells and the densities of immunogold labeling of MnSOD and 4HNE-modified proteins were quantified with image analysis software (Scion Image Beta 4.02, Scion Corp., Frederick, MD, U.S.A.) with a PC computer (Dell OptiPlex GX200). The mean values were obtained from an average of 30 cells from each group.

Statistics

Statistical analyses were performed by paired Student's *t* test or ANOVA. Paired Student's *t* test was used to compare Ntg and TgH mice at each time point. ANOVA with LSD (least significant difference) post-hoc test was used to compare the earliest time point in an individual experiment (0 or 6 h) with later time points. Results were presented as the means ± SEM.

RESULTS

In situ *ultrastructural analysis of mouse skin*

Keratinocytes in mouse skin demonstrated a basal layer adjacent to the basement membrane, an intermediate layer (squamous layer), a more superficial layer (granular layer), and the stratum corneum (Fig. 1a). The stratum corneum was the most superficial layer and consisted of layers of acellular material without cell organelles. Cells from basal, intermediate, and superficial layers had varying numbers of very small but normal-appearing mitochondria with cristae identified (Fig. 1b), and these mitochondria showed immunogold labeling with antibody to MnSOD (Fig. 1c). Mitochondria in skin of mice treated with DMBA/TPA often had injury, as evidenced by the presence of electron-dense mitochondrial inclusions, either single or multiple, with resultant loss of mitochondrial cristae; these inclusions were easily identifiable as round electron-dense structures in material examined by conventional electron microscopy following double staining with lead citrate and uranyl acetate (Fig. 1d). These inclusions were less electron-dense in material prepared for immunogold analysis, at least partially because tissue was stained with uranyl acetate only (Fig. 1e). These inclusions were not observed in untreated mouse skin. One component of these mitochondrial inclusions was lipid peroxidation products, because inclusions were labeled with specific antibody to 4HNE-modified proteins (Fig. 1f). Inclusions were often multiple, resulting in enlargement of mitochondria in comparison with those examined in untreated epidermal cells. Morphologic analysis thus indicated that one major effect of DMBA/TPA treatment was mitochondrial injury, at least partially mediated by lipid peroxidation products reacting with mitochondrial protein(s). The mitochondria with inclusions are probably nonfunctional because cristae cannot be identified.

In situ *analysis of MnSOD immunoreactive protein and cell cycle kinetics in mouse skin*

Previous studies indicated an increase in MnSOD activity in TgH compared with Ntg mouse skin; MnSOD activity in untreated Ntg and TgH mouse skin was determined to be 83 ± 19 and 171 ± 32 units/mg of protein, respectively (39). To determine whether the transgene was properly located in mitochondria of keratinocytes, immunogold analysis was performed. Qualitative studies localized MnSOD immunoreactive proteins in mouse epidermal cells to mitochondria of both TgH and Ntg mice (Fig. 1c). Immunogold morphologic techniques and computerized image analysis were used to quantify MnSOD immunoreactive protein in mouse epidermal cells after DMBA/TPA treatment. Ntg and TgH mice were treated with a single dose of DMBA and 2 weeks later with a single dose of TPA. After mice were killed, the skin was removed and analyzed with quantitative immunogold analysis for levels of MnSOD immunoreactive protein at varying time points after TPA treatment. Immunogold labeling was observed in mitochondria of keratinocytes, but not in significant amounts in other subcellular locations within keratinocytes (Fig. 1c). At all time points examined (6–168 h) in mice treated with DMBA/TPA, there was more MnSOD immunoreactive protein in TgH than Ntg mice (Fig. 2a).

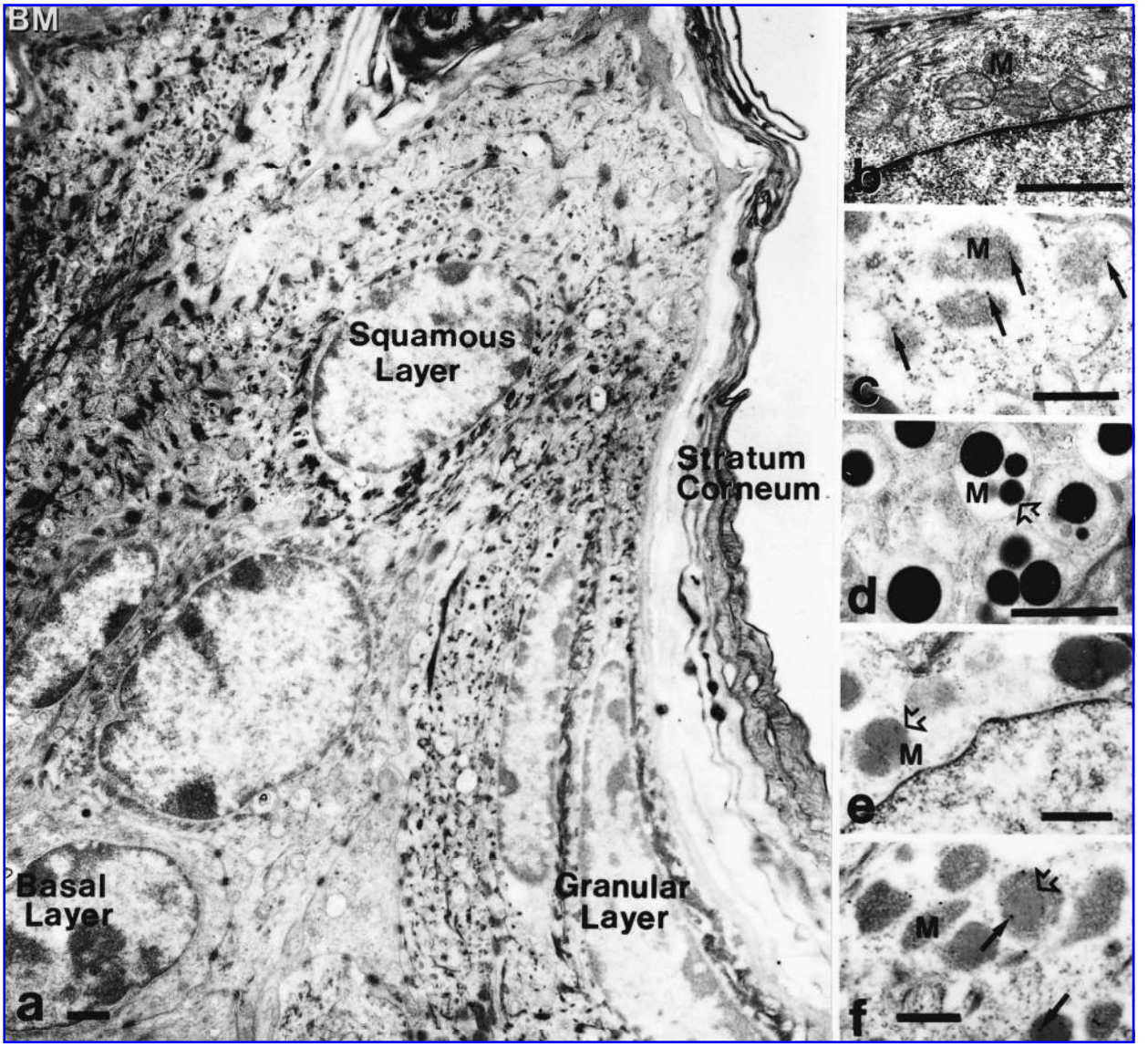

FIG. 1. Ultrastructural analysis of epithelium of normal mouse skin. (a) Conventional electron microscopy of mouse skin, low magnification. Normal mouse skin consists of several layers of keratinocytes, including the basal layer, the squamous layer, the granular layer, and the stratum corneum. Representative cells from these layers are labeled. Basal cells have a cytoplasm with a few mitochondria and a cell surface with tight junctions, and are immediately adjacent to the basement membrane (BM; upper left corner of micrograph); squamous cells have a cytoplasm with prominent tonofilaments, and these tonofilaments converge on tight junctions at the cell surface; and granular cells are similar to squamous cells with the additional feature of cytoplasmic keratohyaline granules. The stratum corneum consists largely of keratin without cell organelles. Mitochondria are very small in normal mouse skin, and so higher magnification is necessary to identify this subcellular organelle. Bar = 1 μm. **(b)** Conventional electron microscopy of epithelium of normal mouse skin, high magnification. Mitochondria (M) of normal mouse skin have normal morphology, with single outer membrane and inner membrane arranged in cristae. However, mitochondria in mouse skin are very small, with only a few cristae. Bar = 1 μm. **(c)** Immunogold electron microscopy of epithelium of normal mouse skin using antibody to MnSOD, high magnifcation. Immunogold label (arrows) was present over mitochondria (M) and not cytoplasm. Bar = 0.5 μm. **(d)** Conventional electron microscopy of epithelium of mouse skin treated with DMBA/TPA, high magnification. Round electron-dense inclusions (double arrow) were identified within mitochondria (M). Mitochondria with inclusions showed loss of cristae. Bar = 1 μm. **(e)** Electron microscopy of epithelium of mouse skin treated with DMBA/TPA, but using same processing as for immunogold electron microscopy, high magnification. Mitochondrial (M) inclusions (double arrow) were identified, but these were much less electron-dense than when conventional microscopy techniques were used, largely because lead citrate was not used as a counterstain. Bar = 0.5 μm. **(f)** Immunogold electron microscopy of epithelium of mouse skin treated with DMBA/TPA and immunostained with antibody to 4HNE-modified proteins. Oxidative damage (immunogold beads identified by single arrows) was present both in mitochondria (M) without morphologic evidence of injury and in mitochondria with inclusions (double arrow). Bar = 0.5 μm.

In addition, the level of MnSOD immunoreactive protein varied significantly as a function of time after DMBA/TPA treatment in TgH but not in Ntg mouse skin (Fig. 2a). In TgH skin, compared with 6-h levels there was a significant decrease in MnSOD immunoreactive protein at 72 h and a subsequent peak in MnSOD immunoreactive protein at 120 h.

Although the 5′-flanking region of the human MnSOD gene promoter has a TPA-responsive element (14), we reasoned that this TPA-responsive element was not responsible for the changes in MnSOD immunoreactive protein in TgH mice because this element was not present in the human MnSOD cDNA used to create the TgH mice. We thus sought an alternative explanation for the variations in MnSOD immunoreactive protein levels observed as a function of time after DMBA/TPA treatment in the TgH mice. As previous studies have demonstrated that TPA induced epidermal cell proliferation (23) and as MnSOD has been demonstrated to vary as a function of growth state (27), we examined mouse skin using conventional electron microscopy. We observed high levels of both mitosis and apoptosis with a peak at 72 h after DMBA/TPA treatment in TgH skin (Fig. 3) in comparison with Ntg skin.

To quantify this observation, mitosis and apoptosis in mouse skin were counted as a function of time after DMBA/TPA treatment using light microscopy and morphologic criteria. There was an increase in both mitosis (Fig. 2b) and apoptosis (Fig. 2c) after DMBA/TPA treatment, and these changes in tissue cell kinetics were much increased in TgH mouse skin in comparison with Ntg mouse skin. Mitosis was increased in TgH mouse skin from 48 to 144 h in comparison with Ntg skin (Fig. 2b). Apoptosis was increased at 72, 96, and 144 h in TgH skin in comparison with Ntg skin (Fig. 2c).

In time-course analyses, in comparison with 6 h after DMBA/TPA treatment, mitosis in TgH mouse skin was elevated at 48–144 h, whereas in Ntg mouse skin, mitosis was elevated only at 72- and 96-h time points (Fig. 2b), but the latter elevations were much less in Ntg than TgH skin. In comparison with 6 h, apoptosis was increased in TgH mouse skin from 48 to 168 h, whereas in Ntg mouse skin apoptosis was increased first at 48–72 h and then again at 168 h, but the latter elevations were much less in Ntg than TgH skin. Control untreated skin had much lower levels of apoptosis than DMBA/TPA-treated mouse skin at the earliest time point

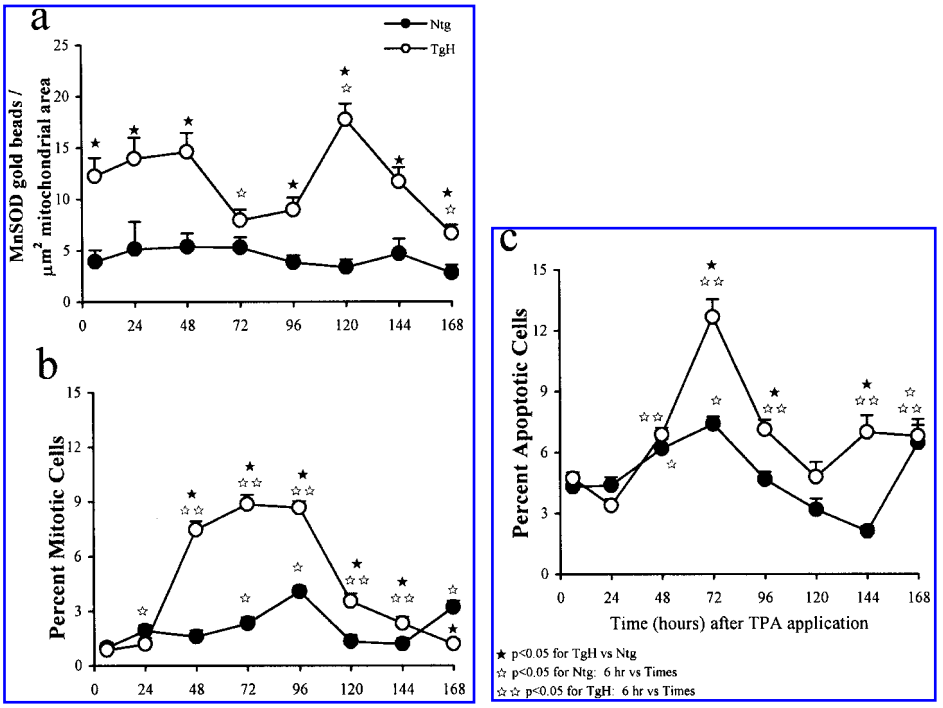

FIG. 2. MnSOD immunoreactive protein in mitochondria and keratinocyte cell kinetics of mouse skin treated with DMBA/TPA. (a) MnSOD immunoreactive protein. At the indicated time points after TPA application following prior DMBA treatment, skin samples were studied with immunogold analysis using specific antibody to MnSOD. Gold beads over mitochondria were quantified, and then image analysis was used to quantify area of mitochondria. Thirty keratinocytes were analyzed per mouse at each time point. Closed stars indicate statistical significance ($p < 0.05$) between TgH and Ntg groups at each time point. Open stars indicate statistical significance ($p < 0.05$) in TgH mice in comparison with 6-h time point. **(b)** Quantitative analysis of mitoses in interfollicular epidermis. Thick sections from the same LR White-embedded material examined in a were analyzed for mitoses using morphologic criteria. Closed stars indicate statistical significance ($p < 0.05$) in comparison of TgH with Ntg mice. Open stars indicate statistical significance ($p < 0.05$) in Ntg mouse skin in comparison of later time points with 6-h time point. Double open stars indicate statistical significance in TgH mouse skin in comparison of later time points with 6-h time point. **(c)** Quantitative analysis of apoptosis in interfollicular epidermis. Thick sections from the same LR White-embedded material examined in a were analyzed for apoptosis using morphologic criteria. Closed stars indicate statistical significance ($p < 0.05$) in comparison of TgH with Ntg mice. Open stars indicate statistical significance ($p < 0.05$) in Ntg mouse skin in comparison of later time points with 6-h time point. Double open stars indicate statistical significance in TgH mouse skin in comparison of later time points with 6-h time point.

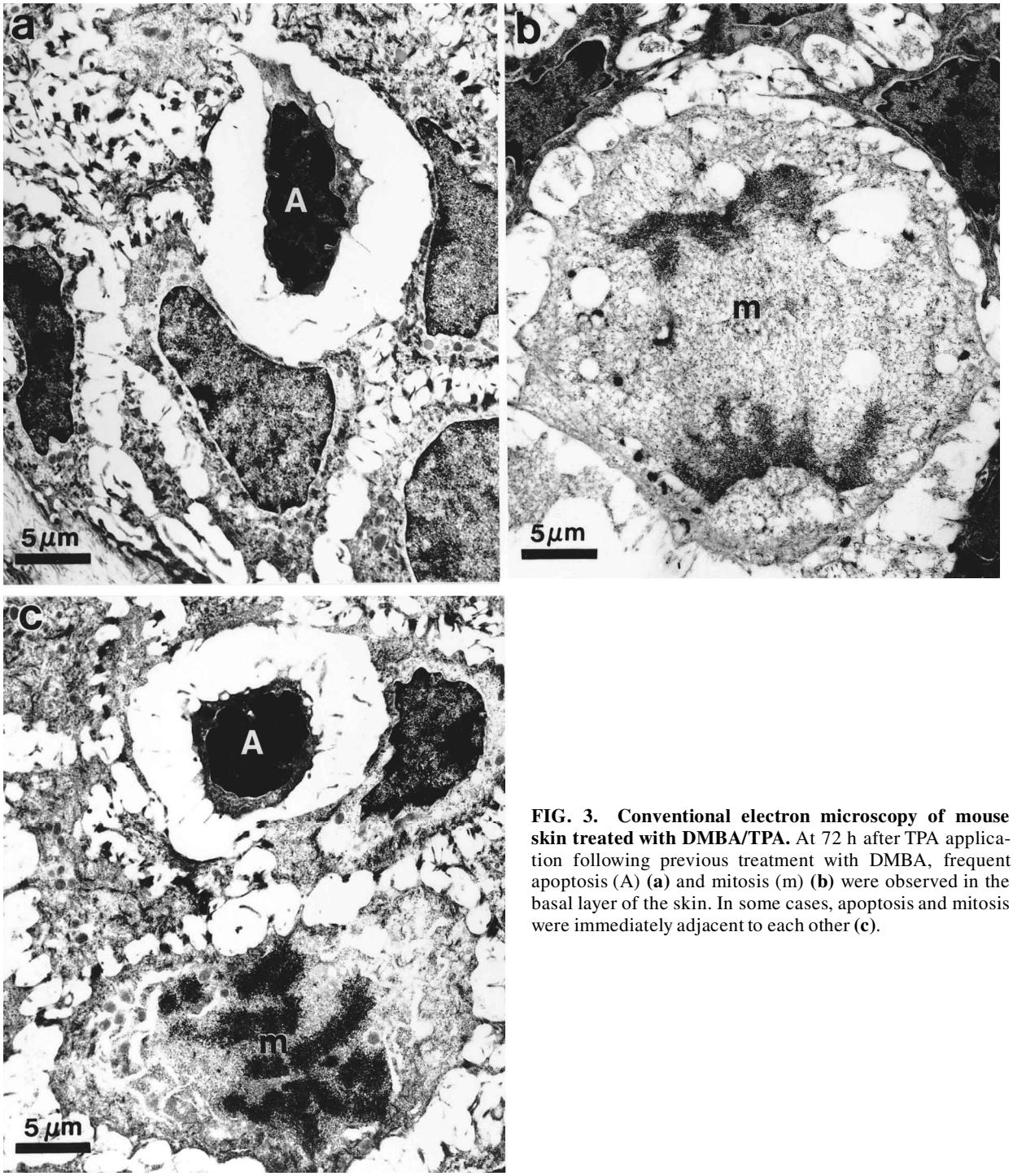

FIG. 3. Conventional electron microscopy of mouse skin treated with DMBA/TPA. At 72 h after TPA application following previous treatment with DMBA, frequent apoptosis (A) **(a)** and mitosis (m) **(b)** were observed in the basal layer of the skin. In some cases, apoptosis and mitosis were immediately adjacent to each other **(c)**.

studied in both Ntg and TgH skin, whereas levels of mitosis in untreated control skin were similar to levels in DMBA/TPA mouse skin at the earliest time point analyzed (compare results at 6 h in Fig. 2b and c with 0-h controls in Table 1).

In mice treated with DMSO alone, DMBA, or TPA (3–48 h), there was more immunoreactive MnSOD in skin of TgH than Ntg mice (data not shown). Untreated control groups had approximately fourfold more MnSOD immunoreactive protein in TgH than Ntg mice (data not shown). These results confirm that, regardless of treatment or time after treatment, TgH mouse keratinocytes expressed more MnSOD immunoreactive protein in mitochondria than keratinocytes from Ntg mice. Our results also demonstrated that MnSOD immunoreactive protein decreased at a time when cell turnover kinetics increased.

In situ *analysis of 4HNE-modified proteins in mouse skin*

To determine how MnSOD overexpression affects lipid peroxidation within the cell, immunogold ultrastructural

TABLE 1. KERATINOCYTE TISSUE KINETICS IN UNTREATED MOUSE SKIN

	Ntg mouse skin	*TgH mouse skin*
Mitosis	0.8 ± 0.5	0.6 ± 0.8
Apoptosis	0.7 ± 0.6	0.6 ± 0.8

*Two Ntg and two TgH mice were studied. LR White-embedded skin was analyzed by light microscopy for mitosis and apoptosis. A total of 1,500 cells were counted per mouse and results expressed as a percentage: mitotic or apoptotic cells/total cells × 100. Results are presented as means ±SEM. Statistical analyses did not reveal significant differences in mitosis or apoptosis in TgH in comparison with Ntg mice.

analysis of keratinocytes was performed using antibody to 4HNE-modified proteins. Consistent with previous studies in rat kidney (37), 4HNE-modified proteins were observed primarily in mitochondria and nucleus, although some cytoplasmic labeling was also evident. Results of quantitative immunogold ultrastructural data and statistical analyses are shown in detail in Fig. 4. Patterns of immunolabeling were very similar in mitochondria and nucleus, but very different in the cytoplasm. In all cases, the trend is toward more 4HNE-modified proteins in Ntg than TgH skin. However, both mitochondria and nucleus show high levels of 4HNE-modified proteins at early time points in both Ntg and TgH mouse skin, whereas this early increase is not noted in the cytoplasm.

Quantitative analysis of skin from DMBA/TPA-treated Ntg mice showed increased levels of 4HNE-modified proteins at 6 and 24 h, but 4HNE-modified proteins declined to levels found in untreated skin (see Fig. 5, time 0 for representative values in untreated skin) at 48 h. In contrast, TgH mice treated with DMBA/TPA demonstrated only a moderate increase in 4HNE-modified protein levels at 6–48 h compared with untreated skin. Comparisons between Ntg and TgH mice treated with DMBA/TPA showed lower levels of 4HNE-modified proteins in mitochondria (Fig. 4a) or nucleus (Fig. 4b) in TgH compared with Ntg mice at early time points, with statistical significance comparing Ntg and TgH achieved in both compartments at 6 h. The cytoplasm showed only low levels of immunolabeling in both Ntg and TgH mouse skin (Fig. 4c), although because of low variability, these levels attained statistical significance; again, TgH in general had lower levels of immunolabeling than Ntg mice.

Keratinocytes from both Ntg and TgH mice treated with DMSO alone or DMBA had only low levels of 4HNE-modified proteins at 3–48 h (data not shown). Detailed results and statistical analysis of mice treated with TPA alone are shown in Fig. 5. Keratinocytes from both Ntg and TgH mice treated with TPA had lower levels of 4HNE-modified proteins at early time points than mice treated with DMBA/TPA (compare Figs. 4 and 5). TgH mice treated with TPA had a baseline level in mitochondria (0 h) of twofold less 4HNE-modified proteins compared with levels in mitochondria of Ntg mice (Fig. 5a). TgH mice showed a further approximate twofold decrease in 4HNE-modified proteins compared with Ntg mice in mitochondria at 3 h after TPA application (Fig. 5a). The nucleus (Fig. 5b) and cytoplasm (Fig. 5c) of keratinocytes treated with TPA also showed a

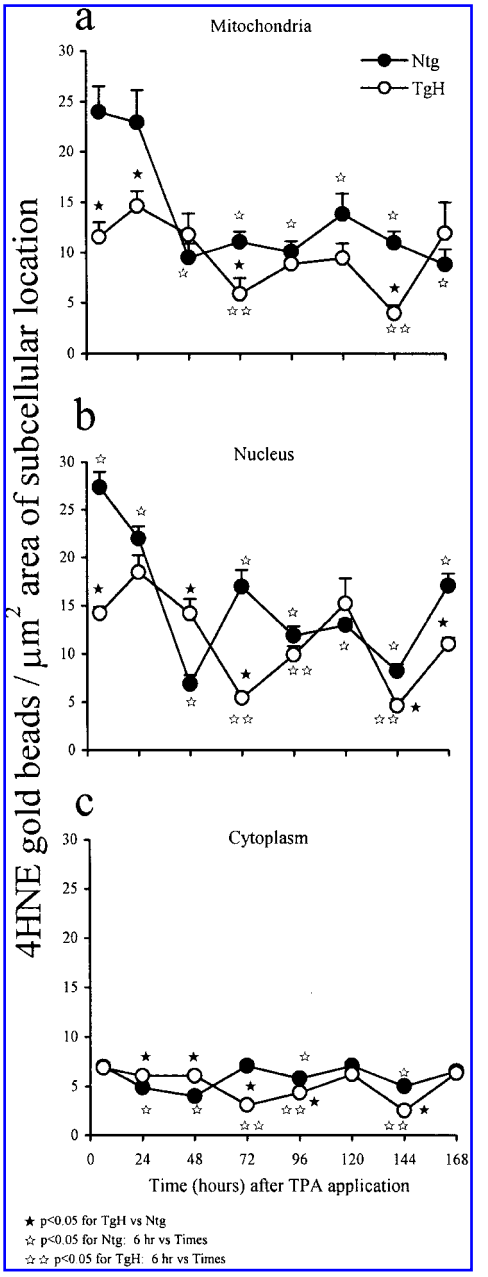

FIG. 4. 4HNE-modified proteins in keratinocytes in mouse skin treated with DMBA/TPA. At the indicated time points after TPA application following prior DMBA treatment, skin samples were analyzed with immunogold techniques using specific antibody to 4HNE-modified proteins. Gold beads over various subcellular compartments (nucleus, mitochondria, and cytoplasm) were quantified, and then image analysis was used to quantify area of each subcellular compartment. Thirty keratinocytes were analyzed per mouse at each time point. **(a)** Gold beads/μm² area of mitochondria. **(b)** Gold beads/μm² area of nucleus. **(c)** Gold beads/μm² area of cytoplasm. Closed stars indicate statistical significance ($p < 0.05$) when comparing each subcellular compartment in skin of TgH with Ntg mice at each time point. Open stars indicate statistical significance ($p < 0.05$) when comparing each subcellular compartment of Ntg mice as a function of time in comparison with 6-h time point. Double open stars indicate statistical significance ($p < 0.05$) when comparing each subcellular compartment of TgH mice as a function of time in comparison with 6-h time point.

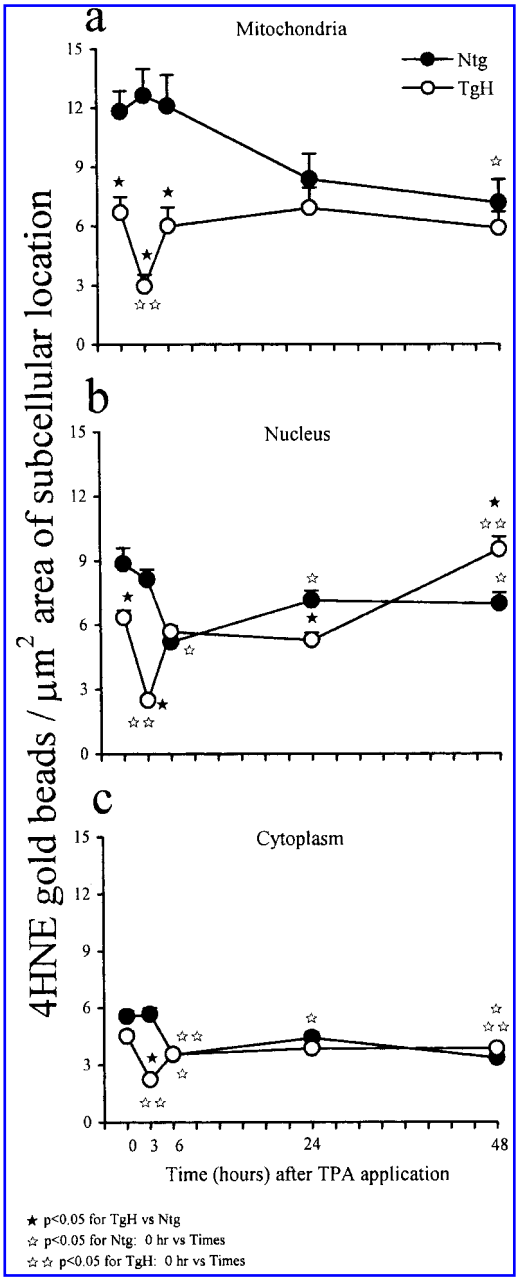

FIG. 5. 4HNE-modified proteins in keratinocytes from mouse skin treated with TPA. At the indicated time points after TPA application, skin samples were analyzed with immunogold techniques using specific antibody to 4HNE-modified proteins. Gold beads over various subcellular compartments (nucleus, mitochondria, cytoplasm) were quantified, and then image analysis was used to quantify area of each subcellular compartment. Thirty keratinocytes were analyzed per mouse at each time point. **(a)** Gold beads/μm² of mitochondria. **(b)** Gold beads/μm² of nucleus. **(c)** Gold beads/μm² of cytoplasm. Closed stars indicate statistically significant ($p < 0.05$) differences when comparing each subcellular compartment in skin of TgH with Ntg mice at each time point. Open stars indicate statistical significance ($p < 0.05$) when comparing each subcellular compartment of Ntg mice as a function of time in comparison with 0-h control. Double open stars indicate statistical significance ($p < 0.05$) when comparing each subcellular compartment of TgH mice as a function of time in comparison with 0-h control.

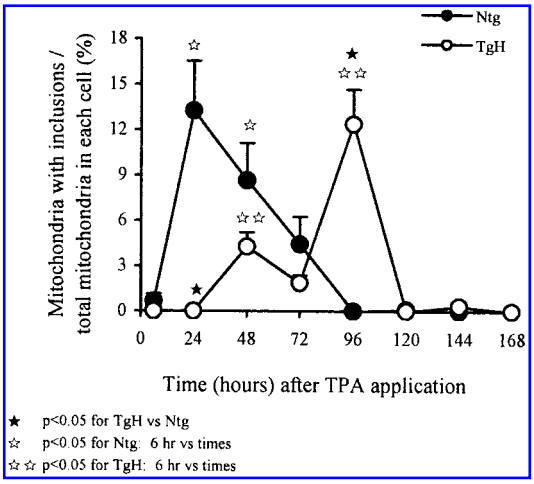

FIG. 6. Mitochondrial inclusions in keratinocytes from mouse skin treated with DMBA/TPA. At the indicated time points after TPA application following DMBA treatment, skin samples were analyzed for mitochondrial inclusions. Results are expressed as percentage of total mitochondria. Closed stars indicate statistically significant differences ($p < 0.05$) when comparing skin of TgH and Ntg at each time point. Open stars indicate statistical significance ($p < 0.05$) when comparing mitochondrial inclusion percentage in Ntg mice as a function of time in comparison with 6-h time point. Double open stars indicate statistical significance ($p < 0.05$) when comparing mitochondrial inclusion percentage in TgH mice as a function of time in comparison with 6-h time point.

significant decrease in lipid peroxidation-protein adducts at 3 h in TgH compared with Ntg mice, but these decreases were less than those observed in mitochondria.

Mitochondrial injury is delayed in TgH mice

Detailed results and statistical analyses of mitochondrial inclusion formation in Ntg and TgH mouse skin are presented in Fig. 6. Mitochondrial inclusions expressed as a percentage of total mitochondria peaked at 24 h in Ntg mice, but at 96 h in TgH mice. At early time points (24 h) in keratinocytes from TgH mice, there were no inclusions identified, whereas keratinocytes from Ntg mice had a significant number of inclusions at this time point. Mitochondria with inclusions demonstrated loss of cristae (Fig. 1d). Mice treated with DMBA alone did not show inclusions (data not shown).

DISCUSSION

The present study documents that overexpression of a mitochondrial antioxidant enzyme, MnSOD, can have profound effects not only on mitochondrial injury, but also on events occurring elsewhere in the cell, *i.e.*, the nucleus. A previous study has documented that overexpression of MnSOD in mice reduced papilloma incidence two- to threefold (39). This same study showed decreases in immunoreactive protein levels of PKCϵ, JNKinase, and Jun D and a decrease in the activity of nuclear transcription factor AP-1 following DMBA/TPA treat-

ment in skin of TgH compared with Ntg mice. These results demonstrated that overexpression of a mitochondrial enzyme can affect proteins present in the nucleus (Jun D) and cytoplasm (JNKinase). Because ROS are able to function as signal mediators, it is possible that MnSOD achieves these pleiotropic effects by affecting cell redox state, thus affecting mitochondria-to-nucleus signaling pathways. In turn, mitochondria-to-nucleus signaling pathways have been shown to be responsible for induction of MnSOD by tumor necrosis factor-α (32).

The present study documents that the MnSOD overexpression that occurs in TgH mice was detectable to an appreciable extent only in mitochondria. Previous studies analyzing skin homogenates with activity gels have demonstrated increased MnSOD activity in TgH compared with Ntg skin, and biochemical analysis has shown an approximate twofold increase in activity (39). Although the present study measured only MnSOD immunoreactive protein, immunogold beads were not found in significant amounts in any subcellular location other than mitochondria, indicating that the increase in MnSOD activity in skin homogenates in TgH compared with Ntg mice must be primarily due to an increase in mitochondrial activity. Therefore, biochemical and biologic effects observed in TgH mice must be due to biochemical effects of MnSOD overexpression in mitochondria.

How mitochondrial events affect whole cell behavior is a subject of great interest. The p53 tumor suppressor protein can act as a transcription factor and cause cell cycle arrest when it is located in the nucleus; however, when cells are oxidatively damaged, this protein can translocate to mitochondria, resulting in apoptosis (21). Another protein that functions in mitochondria is Bcl-2. *Bcl-2* was originally identified as a human lymphoma oncogene. A growing body of evidence indicates that the crucial site of Bcl-2 action appears to be the mitochondria (8). Interestingly, Bcl-2 is able to inhibit the apoptotic effects of p53. Recently, it has been demonstrated that Ras may localize to mitochondria to effect apoptosis, and the apoptotic effect of Ras is blocked by Bcl-2 (6). As it is known that mutated *ras* is a primary initiation event in papilloma formation (23) and it is known that oncogenic *ras* leads to the production of oxygen radicals (19), it is tempting to speculate that MnSOD overexpression prevents papilloma formation by blocking the effects of Ras-mediated ROS formation. Future studies will be necessary to test this exciting hypothesis.

Numerous studies have demonstrated that MnSOD has pleiotropic effects on cells. In a cell culture model, we have demonstrated that MnSOD suppressed radiation-induced neoplastic transformation (33). In two other cell culture models, we showed that MnSOD overexpression promoted cellular differentiation (34, 40). We have demonstrated that MnSOD overexpression can inhibit apoptosis secondary to injurious stimuli (20). A recent study has documented that MnSOD overexpression using MnSOD cDNA transfection can result in apoptosis in noninjured cells (30). We have shown that MnSOD overexpression inhibits cell cycle progression in tissue culture models (16, 17). MnSOD has also been demonstrated to protect cells from oxidative stress during quiescence (15). Thus, results of MnSOD overexpression have many effects on cell behavior, which may in turn depend on cell type and physiologic and pathologic variables not yet well understood. The present study is the first to study effects of MnSOD overexpression on cell kinetics *in situ* and clearly demonstrates that MnSOD overexpression affects both cell birth and cell death after injury. How MnSOD regulates these complex processes is a subject of great importance. The above results imply mitochondria-to-nucleus signaling events as important regulators of cell function.

The biologic effects of MnSOD on cells are complex for many reasons. First, the enzyme converts superoxide anion into hydrogen peroxide. Normally, hydrogen peroxide is removed by either catalase or glutathione peroxidase. However, in cases where hydrogen peroxide is not completely removed, alterations in cell redox state will occur, resulting in modifications of redox-sensitive proteins, *i.e.*, transcription factors [AP-1, nuclear factor-κB, (NF-κB), p53, etc.] and proteins involved in signal transduction pathways (24). Second, MnSOD is induced at the transcriptional level by several factors, including ROS, cytokines (32), and TPA (14). Third, MnSOD is regulated by transcription factors that are redox-sensitive [cRel (2), p53 (41)], resulting in reciprocal regulation. NF-κB has been demonstrated to both positively and negatively regulate proliferation and apoptosis, and it has been shown in HeLa cells that MnSOD activity is crucial in effecting these decisions induced by NF-κB (2). Finally, MnSOD has both physiologic [regulation of mitochondrial redox state, mitochondrial function (16), and regulation of cell cycle progression (20)] and pathologic functions [protection against ROS, induction of apoptosis]. Thus, MnSOD is critical in regulating cell behavior.

It seems paradoxical that MnSOD may both protect against and promote apoptosis. The simplest explanation for these apparent discrepant findings (protection versus apoptosis) is that the effects of MnSOD modulation in cell behavior are dependent on changes in cell redox state, which can be oxidizing or reducing depending on the unique biochemistry of each cell type, including the ability of each cell type to adapt to increased hydrogen peroxide formation generated by the enzymatic function of MnSOD. In fact, our laboratory has directly demonstrated that overexpression of high levels of MnSOD in mouse fibroblasts using an adenoviral vector system results in cell death, which correlates with increasing ROS levels and altered redox levels as assessed by glutathione/glutathione disulfide ratios (13).

Levels of 4HNE-modified proteins were increased compared with those of controls at early time points after TPA treatment in mice previously treated with DMBA. Localization of this oxidative damage product was primarily in mitochondria and nucleus. Epidermal cells from TgH mice treated with DMBA/TPA had much less oxidative damage than corresponding epidermal cells from Ntg mice. These results demonstrated that DMBA/TPA treatment caused oxidative damage in both nucleus and mitochondria, and MnSOD overexpression was able to protect against this damage in both locations. Keratinocytes from Ntg mice treated with TPA alone exhibited significant levels of mitochondrial lipid peroxidation-protein adducts, but less nuclear and cytoplasmic lipid peroxidation-protein adducts. These results imply that TPA-mediated oxidative damage is primarily mitochondrial. Lipid peroxidation-modified proteins were lower at early time points in TPA- compared with DMBA/TPA-treated mice in all

subcellular locations, suggesting that DMBA/TPA is more oxidative than TPA alone. Levels of 4HNE-modified proteins in TgH mice treated with TPA were significantly reduced in all subcellular compartments, again suggesting that overexpression of MnSOD can affect redox status throughout the cell. It is not certain how MnSOD causes these changes, but possibilities include modulated diffusion of hydrogen peroxide and/or lipid hydroperoxides throughout the cell and/or direct effects on cell signaling pathways. It has been recently demonstrated that overexpression of catalase in either mitochondria or cytosol was equally protective against oxidants generated in mitochondria by rotenone or antimycin A (1). These data suggest that hydrogen peroxide readily diffuses into the cytosol. As it has been shown that treatment with high concentrations of DMBA alone can cause oxidative stress (9), our data are consistent with the hypothesis that DMBA and TPA are synergistic in causing oxidative damage.

To our knowledge, mitochondrial inclusions have not been identified previously in a multistage carcinogenesis model. A literature search did not reveal similar inclusions in other experimental or human cancers. We have identified these inclusions in early preneoplastic skin lesions (11) in other strains of mice that have been treated with DMBA/TPA (unpublished observations), which suggests the possibility that these lesions are associated with cancer formation. In the present model, the inclusions are transient because inclusions are no longer present 120 h after TPA treatment in both Ntg and TgH mice, but are delayed in TgH compared with Ntg mice. It is not known whether the inclusion-containing mitochondria are degraded or repaired. It has been previously demonstrated that overexpression of cRel transcription factor in cultured cells caused an increase in MnSOD levels, resulting in oxidative damage, presumably due to hydrogen peroxide production via the enzymatic activity of MnSOD, and injury to mitochondria (3). Interestingly, these injured mitochondria were subsequently degraded by lysosomes, resulting in the formation of lipofuscin. Previous studies in our laboratory have demonstrated that lipofuscin contains 4HNE-protein adducts (29), suggesting the possibility that the mitochondrial inclusions identified in the skin in the present study will be eventually degraded by lysosomes to lipofuscin. The delay in appearance of these inclusions in TgH compared with Ntg mice suggests a role for ROS in their development, and, indeed, these lesions contain 4HNE-modified proteins (Fig. 1f). 4HNE-modified proteins peaked between 6 and 24 h in Ntg mice, and mitochondrial inclusions reached a maximum at 24 h, showing good correlation. 4HNE-modified proteins are elevated above control until 48 h in TgH mice, a time at which inclusions first begin to appear. Thus, in both Ntg and TgH mice, 4HNE-modified protein levels parallel inclusion formation, suggesting the possibility that lipid peroxidation is causal in inclusion formation. The facts that application of SOD mimics (7) and overexpression of MnSOD both inhibit papilloma formation strongly implicate ROS in their genesis. Another group has demonstrated the *in vitro* reaction of 4HNE with mitochondrial proteins in a study of isolated mitochondria using western analysis (5).

There are some inherent difficulties with the immunomorphologic techniques utilized in the present study. Large numbers of samples to be stained at the same time is a limiting factor. Thus, the experiments outlined herein were performed in two groups: (a) DMBA/TPA, DMBA, and DMSO alone, and (b) TPA and DMSO alone. This creates potential problems with analysis of immunogold results, because accurate analyses depend on precise fixation, embedding, and staining. Using parallel biochemical measurements, we have demonstrated that immunogold results are sensitive, specific, and reproducible when all tissues are processed at the same time (37, 38). Each of the two groups analyzed above had a common group, *i.e.*, mice treated with DMSO alone as control, and quantitative results from these two sets of DMSO-treated mice were nearly identical. Therefore, we are confident that the results from other treatment groups described above are directly comparable.

There was variation in levels of MnSOD immunoreactive protein (approximate twofold differences at maximal and minimal levels) as a function of time after TPA treatment in TgH mice, and statistical analysis showed these variations to be significant. These variations may reflect biochemical changes associated with mitosis after TPA application. As mentioned previously, *in vitro* studies in our laboratory have demonstrated variations in ROS and antioxidant enzymes during the cell cycle in mammalian cells (16, 17, 27). Serum starvation studies in NIH/3T3 fibroblasts have shown that MnSOD levels decrease as quiescent cells enter the cell cycle (27). Studies in synchronized NIH/3T3 fibroblasts and DU145 prostate carcinoma cells showed a decrease in MnSOD activity in S but not M phases of the cell cycle (16, 18). The decrease in MnSOD immunoreactive protein observed in the present study may be at least partially due to increased cells in S phase of the cell cycle. However, as the transgene was constructed with a β-actin promoter, the changes in MnSOD could also be due to changes in actin levels as a result of altered cell tissue kinetics. Previous studies have demonstrated that MnSOD levels increase in many epithelial cell types during development and differentiation (25). The increase in MnSOD immunoreactive protein at 120 h following DMBA/TPA treatment is most likely due to cell differentiation following unscheduled mitosis.

The present study documents a time course of biochemical and morphologic events in DMBA/TPA-treated mouse skin. A single dose of TPA following prior DMBA treatment results in lipid peroxidation at 6 h, with less lipid peroxidation in the MnSOD TgH mice. Mitochondrial inclusions occurred at 24 h in Ntg mice and 96 h in TgH mice. Alterations in keratinocyte cell kinetics occur at 48 h in both types of mice, although TgH mice showed increased levels of both mitosis and apoptosis in comparison with Ntg mice. A future study of importance is whether initiated cells in MnSOD-overexpressing mice are differentially sensitive to apoptosis, thus explaining the decrease in papilloma formation in TgH mice.

In summary, the present study demonstrates for the first time in intact skin that overexpression of the mitochondrial antioxidant enzyme MnSOD protects not only the mitochondria, but also the nucleus from lipid peroxidation. The manner by which this is achieved will be studied in our laboratory and should prove to be of considerable interest. The present study also demonstrates that DMBA/TPA treatment affects cell turnover kinetics and results in mitochondrial injury in treated mouse skin; which or both of these effects results in decreased papilloma formation in MnSOD-overexpressing mice will be the subject of future studies.

ACKNOWLEDGMENTS

The authors would like to thank Ms. Jamie McMaster for technical assistance. The authors would also like to thank Ms. Jamie McMaster for editing and Dr. Larry Oberley for critical reading of the manuscript. This work was supported by NIH grants CA73599 and CA73599-S2. This work was supported with resources and use of facilities at the Department of Veterans Affairs Medical Center, Madison, WI.

ABBREVIATIONS

AP-1, activator protein-1; DMBA, 7,12-dimethylbenz(*a*)-anthracene; DMSO, dimethyl sulfoxide; 4HNE, 4-hydroxy-2-nonenal; MnSOD, manganese-containing superoxide dismutase; NF-κB, nuclear factor-κB; Ntg, nontransgenic; PKC, protein kinase C; ROS, reactive oxygen species; SOD, superoxide dismutase; TBS, Tris-buffered saline; TgH, transgenic; TPA, 12-*O*-tetradecanoylphorbol 13-acetate.

REFERENCES

1. Bai J, Rodriguez AM, Melendez JA, and Cederbaum AI. Overexpression of catalase in cytosolic or mitochondrial compartment protects Hep G2 cells against oxidative injury. *J Biol Chem* 274: 26217–26224, 1999.
2. Bernard D, Quatannens B, Begue A, Vandenbunder B, and Abbadie C. Antiproliferative and antiapoptotic effects of cRel may occur within the same cell via the up-regulation of manganese superoxide dismutase. *Cancer Res* 61: 2656–2664, 2001.
3. Bernard D, Slomianny C, Vandenbunder B, and Abbadie C. cRel induces mitochondrial alterations in correlation with proliferation arrest. *Free Radic Biol Med* 31: 943–953, 2001.
4. Boutwell RK. The function and mechanism of promoters of carcinogenesis. In: *CRC Critical Reviews in Toxicology*, edited by Goldberg, L. Cleveland, OH: CRC Press Inc., 1974, pp. 419–443.
5. Cohn J, Tsai L, and Szweda LI. Structural identification of 4-hydroxy-2-nonenal-protein cross-link and immunochemical detection in mitochondria exposed to oxidative stress. *Arch Biochem Biophys* 328: 158–164, 1996.
6. Denis GV, Yu Q, Ma P, Deeds L, Faller DV, and Chen C-Y. Bcl-2, via its BH4 domain, blocks apoptotic signaling mediated by mitochondrial ras. *J Biol Chem* 278: 5775–5785, 2003.
7. Egner PA and Kensler TW. Effects of a biomimetic superoxide dismutase on complete and multistage carcinogenesis in mouse skin. *Carcinogenesis* 6: 1167–1172, 1985.
8. Esposti MD, Hatzinisiriou I, McLennan H, and Ralph S. Bcl-2 and mitochondrial oxygen radicals: new approaches with reactive oxygen species-sensitive probes. *J Biol Chem* 274: 29831–29837, 1999.
9. Frenkel K, Wei L, and Wei H. 7,12-Dimethylbenz[*a*]anthracene induces oxidative DNA modification in vivo. *Free Radic Biol Med* 19: 373–380, 1995.
10. Gonzalez A, Oberley TD, and Li JJ. Morphological and immunohistochemical studies of the estrogen-induced Syrian hamster renal tumor: probable cell of origin. *Cancer Res* 49: 1020–1028, 1989.
11. Jansen AP, Dreckschmidt NE, Verwiebe EG, Wheeler DL, Oberley TD, and Verma AK. Protein kinase C epsilon transgenic mice: a unique model for metastatic squamous cell carcinoma. *Cancer Res* 61: 808–812, 2001.
12. Kikawa U, Takai Y, Tanaka Y, Miyake R, and Nishizuka Y. Protein kinase C as a possible receptor protein of tumor-promoting phorbol esters. *J Biol Chem* 258: 11442–11445, 1983.
13. Kim AK, Oberley LW, and Oberley TD. Inhibition of cell growth by MnSOD overexpression in human fibroblasts. Ninth Annual Meeting of the Oxygen Society, Abstract no. 314, 2002.
14. Kim H-P, Roe J-H, Chock PB, and Yim KB. Transcriptional activation of the human manganese superoxide dismutase gene mediated by tetradecanoylphorbol acetate. *J Biol Chem* 274: 37455–37460, 1999.
15. Kops JPL, Dansen TB, Polderman PE, Saarloos I, Wirtz KWA, Coffer PJ, Huang T-T, Bos JL, Medema RJ, and Burgering BMT. Forkhead transcription factor FOXO3a protects quiescent cells from oxidative stress. *Nature* 419: 316–321, 2002.
16. Li N and Oberley TD. Modulation of antioxidant enzymes, reactive oxygen species, and glutathione levels in manganese superoxide dismutase-overexpressing NIH/3T3 fibroblasts during the cell cycle. *J Cell Physiol* 177: 148–160, 1998.
17. Li N, Oberley TD, Oberley LW, and Zhong W. Inhibition of cell growth in NIH/3T3 fibroblasts by overexpression of manganese superoxide dismutase: mechanistic studies. *J Cell Physiol* 175: 359–369, 1998.
18. Li N, Zhai Y, and Oberley TD. Two distinct mechanisms for inhibition of cell growth in human prostate carcinoma cells with antioxidant enzyme imbalance. *Free Radic Biol Med* 26: 1554–1568, 1999.
19. Liou JS, Chen CY, Chen JS, and Faller DV. Oncogenic *ras* mediates apoptosis in response to protein kinase C inhibition through the generation of reactive oxygen species. *J Biol Chem* 275: 39001–39011, 2000.
20. Majima HJ, Oberley TD, Furukawa K, Mattson MP, Yen H-C, Szweda LI, and St. Clair DK. Prevention of mitochondrial injury by manganese superoxide dismutase reveals a primary mechanism for alkaline-induced cell death. *J Biol Chem* 273: 8217–8224, 1998.
21. Marchenko ND, Zaika A, and Moll UM. Death signal-induced localization of p53 protein to mitochondria: a potential role in apoptotic signaling. *J Biol Chem* 275: 16202–16212, 2000.
22. Morris RJ, Tryson KA, and Wu KQ. Evidence that the epidermal targets of carcinogen action are found in the interfollicular epidermis or infundibulum as well as in the hair follicles. *Cancer Res* 60: 226–229, 2000.
23. Mukhtar H, Mercurio MC, and Agarwal R. Skin carcinogenesis: relevance to humans. In: *Skin Cancer: Mechanisms and Human Relevance*, edited by Mukhtar H. Boca Raton, FL: CRC Press, 1995, pp. 3–8.
24. Oberley TD. Oxidative damage and cancer. *Am J Pathol* 160: 403–408, 2002.
25. Oberley TD, Oberley LW, Slattery AF, Lauchner LJ, and Elwell JH. Immunohistochemical localization of antioxi-

dant enzymes in adult Syrian hamster tissues and during kidney development. *Am J Pathol* 137: 199–214, 1990.
26. Oberley TD, Sempf JM, Oberley MJ, McCormick ML, Muse KE, and Oberley LW. Immunogold analysis of antioxidant enzymes in human renal carcinoma. *Virchows Archiv* 424: 155–164, 1994.
27. Oberley TD, Schultz JL, Li N, and Oberley LW. Antioxidant enzyme levels as a function of growth state in cell culture. *Free Radic Biol Med* 19: 53–65, 1996.
28. Oberley TD, Toyokuni S, and Szweda LI. Localization of hydroxynonenal protein adducts in normal human kidney and selected human kidney cancers. *Free Radic Biol Med* 27: 695–703, 1999.
29. Oberley TD, Zhong W, Szweda LI, and Oberley LW. Localization of antioxidant enzymes and oxidative damage products in normal and malignant prostate epithelium. *Prostate* 44: 144–155, 2000.
30. Plymate SR, Haugk KH, Sprenger CC, Nelson PS, Tennant MK, Zhang Y, Oberley LW, Zhong W, Drivdahl R, and Oberley TD. Increased manganese superoxide dismutase (SOD-2) is part of the mechanism for prostate tumor suppression by Mac 25/insulin-like growth factor binding protein-related protein-1. *Oncogene* 22: 1024–1034, 2003.
31. Robertson FM, Beavis AJ, Oberyszyn TM, O'Connell TM, Dokidos A, Laskin DL, Laskin JD, and Reiners JJ. Production of hydrogen peroxide by murine epidermal keratinocytes following treatment with the tumor promoter 12-*O*-tetradecanoylphorbol13-acetate. *Cancer Res* 58: 6062–6067, 1990.
32. Rogers RJ, Monnier JM, and Nick HS. Tumor necrosis factor-α selectively induces MnSOD expression via mitochondria-to-nucleus signaling, whereas interleukin-1β utilizes an alternative pathway. *J Biol Chem* 276: 20419–20427, 2001.
33. St. Clair DK, Wan XS, Oberley TD, Muse KE, and St. Clair WH. Suppression of radiation-induced neoplastic transformation by overexpression of mitochondrial superoxide dismutase. *Mol Carcinog* 6: 238–242, 1992.
34. St. Clair DK, Oberley TD, Muse KE, and St. Clair WH. Expression of manganese superoxide dismutase promotes cellular differentiation. *Free Radic Biol Med* 16: 275–282, 1994.
35. Wheeler DL, Ness KJ, Oberley TD, and Verma AK. Inhibition of the development of metastatic squamous cell carcinoma in protein kinase C epsilon transgenic mice by α-difluoromethylornithine accompanied by marked hair follicle degeneration and hair loss. *Cancer Res* 63: 3037–3042, 2003.
36. Yen HC, Oberley TD, Vichitbandha S, Ho YS, and St. Clair DK. The protective role of manganese superoxide dismutase against adriamycin-induced acute cardiac toxicity in transgenic mice. *J Clin Invest* 98: 1253–1260, 1996.
37. Zainal TA, Weindruch R, Szweda LI, and Oberley TD. Localization of 4-hydroxy-2-nonenal modified proteins in kidney following iron overload. *Free Radic Biol Med* 26: 1181–1193, 1999.
38. Zainal TA, Oberley TD, Allison DB, Szweda LI, and Weindruch R. Caloric restriction of rhesus monkeys lowers oxidative damage in skeletal muscle. *FASEB J* 14: 1825–1836, 2000.
39. Zhao Y, Xue Y, Oberley TD, Kiningham KK, Lin S, Yen H-C, Majima H, Hines J, and St. Clair DK. Overexpression of MnSOD suppresses tumor formation by modulation of AP-1 signaling in a multistage skin carcinogenesis model. *Cancer Res* 61: 6082–6088, 2001.
40. Zhao Y, Kiningham KK, Lin S-M, and St. Clair DK. Overexpression of MnSOD protects murine fibrosarcoma cells (Fsa-II) from apoptosis and promotes a differentiation program upon treatment with 5-azacytidine: involvement of MAPK and NFκB pathways. *Antioxid Redox Signal* 3: 375–386, 2001.
41. Zhao Y, Oberley TD, Chaiswing L, Lin S, Epstein CJ, Huang TT, and St. Clair DK. Manganese superoxide dismutase deficiency enhances cell turnover via tumor-promoter-induced alterations in AP-1 and p53-mediated pathways in a skin cancer model. *Oncogene* 21: 3836–3846, 2002.

Address reprint requests to:
Terry D. Oberley
William S. Middleton Veterans Memorial Hospital, Room A35
2500 Overlook Terrace
Madison, WI 53705

E-mail: toberley@facstaff.wisc.edu
or
Daret St. Clair
University of Kentucky
454 Health Sciences Research Building
Lexington, KY 40536

E-mail: dstcl00@pop.uky.edu

Received for publication October 7, 2003; accepted February 19, 2004.

This article has been cited by:

1. Sanjit Kumar Dhar, Daret K. St. Clair. 2012. Manganese superoxide dismutase regulation and cancer. *Free Radical Biology and Medicine* **52**:11-12, 2209-2222. [CrossRef]
2. V. A. Kobliakov. 2010. Mechanisms of tumor promotion by reactive oxygen species. *Biochemistry (Moscow)* **75**:6, 675-685. [CrossRef]
3. Ae-Kyong Kim. 2010. Modulation of MnSOD in Cancer: Epidemiological and Experimental Evidences. *Toxicological Research* **26**:2, 83-93. [CrossRef]
4. Joydeb Kumar Kundu, Eun-Jin Chang, Hajime Fujii, Buxiang Sun, Young-Joon Surh. 2008. Oligonol Inhibits UVB-induced COX-2 Expression in HR-1 Hairless Mouse Skin—AP-1 and C/EBP as Potential Upstream Targets. *Photochemistry and Photobiology* **84**:2, 399-406. [CrossRef]
5. Aldo Mancini, Antonella Borrelli, Antonella Schiattarella, Stefania Fasano, Antonella Occhiello, Alessandra Pica, Peter Sehr, Massimo Tommasino, Jürg P.F. Nüesch, Jean Rommelaere. 2006. Tumor suppressive activity of a variant isoform of manganese superoxide dismutase released by a human liposarcoma cell line. *International Journal of Cancer* **119**:4, 932-943. [CrossRef]
6. Dr. Shinya Toyokuni . 2006. Novel Aspects of Oxidative Stress-Associated Carcinogenesis. *Antioxidants & Redox Signaling* **8**:7-8, 1373-1377. [Abstract] [Full Text PDF] [Full Text PDF with Links]
7. Terry D. Oberley . 2004. Mitochondria, Manganese Superoxide Dismutase, and Cancer. *Antioxidants & Redox Signaling* **6**:3, 483-487. [Citation] [Full Text PDF] [Full Text PDF with Links]
8. Aekyong Kim , Weixiong Zhong , Terry D. Oberley . 2004. Reversible Modulation of Cell Cycle Kinetics in NIH/3T3 Mouse Fibroblasts by Inducible Overexpression of Mitochondrial Manganese Superoxide Dismutase. *Antioxidants & Redox Signaling* **6**:3, 489-500. [Abstract] [Full Text PDF] [Full Text PDF with Links]